Cellulose (2022) 29:5745–5763
https://doi.org/10.1007/s10570-022-04629-z

ORIGINAL RESEARCH

Green, ultrafine cellulose-based porous nanofibrous membranes for efficient heavy metal removal through incorporation of chitosan by various electrospinning ways

Jiaxi Wu · Qiushi Li · Ganmao Su · Ronggang Luo · Duanben Du · Linkun Xie · Zhengguan Tang · Jinsong Yan · Juying Zhou · Siqun Wang · Kaimeng Xu

Received: 29 December 2021 / Accepted: 27 April 2022 / Published online: 23 May 2022

Abstract Rapid global industrialization has worsened the heavy metal contamination of aquatic ecosystems globally. In this study, green, ultrafine cellulose-based porous nanofibrous membranes for efficient heavy metal removal were obtained by incorporating chitosan (CS) and using conventional and core–shell electrospinning ways. The relationship between the parameters of the electrospinning solution, the micro-morphology and porosity, the chemically active sites, the thermal stability, and the adsorption performance of the biocomposite nanofibrous membranes were analyzed. The adsorption effects of the copper ions, including the initial concentration, solution pH, and interaction time, were investigated. The results show that the average diameters of the conventional and core–shell ultrafine nanofibers with 50% and 30% CS loading are 56.22 nm and 37.28 nm, respectively. The core–shell cellulose acetate (CA)/CS biocomposite nanofibrous membranes showed the weaker thermal stability with a 48.2 °C lower maximum thermal decomposition temperature and induced the surface aggregation of more copper ions compared to the conventional one. A more uniform distribution of the chemical adsorption sites is obtained by conventional single-nozzle electrospinning than by core–shell electrospinning, which effectively promotes the adsorption performance of copper ions and decreases the surface shrinkage of the nanofibrous membranes during adsorption. The 30% CS conventional nanofibrous membranes at an aqueous solution pH of 5 showed the optimum adsorption capacity of copper ions (86.4 mg/g). The smart combination of renewable biomass with effective chemical adsorption sites, electrospinning technology that produces an interwoven porous structure, and an adsorption method with low cost and facile operation shows a promising prospect for water treatment.

J. Wu · G. Su · R. Luo · D. Du · L. Xie · K. Xu (✉)
International Joint Research Center for Biomass Materials, Ministry of Science and Technology, Southwest Forestry University, Kunming 650224, People's Republic of China
e-mail: xukm007@163.com

J. Wu · Q. Li · R. Luo · D. Du · L. Xie · J. Yan · K. Xu
Yunnan Provincial Key Laboratory of Wood Adhesives and Glued Products, Southwest Forestry University, Kunming 650224, People's Republic of China

Z. Tang
School of Chemical and Biomolecular Engineering, Georgia Institute of Technology, Atlanta, GA 30332, USA

J. Zhou
Key Laboratory of Chemistry and Engineering of Forest Products, State Ethnic Affairs Commission; Guangxi Key Laboratory of Chemistry and Engineering of Forest Products, Guangxi Minzu University, Nanning 530006, People's Republic of China

S. Wang (✉)
Center for Renewable Carbon, The University of Tennessee, Knoxville, TN 37996, USA
e-mail: swang@utk.edu

Keywords Ultrafine nanofibrous membranes · Electrospinning · Cellulose acetate · Chitosan · Adsorption · Copper ions

Introduction

The rapid development of global industrialization has led to a worsening pollution crisis of aquatic ecosystems (Cheng et al. 2021; Sun et al. 2022). Increases in heavy metal concentrations in global water resources resulting from industrial and agricultural wastes, natural weathering of crustal rocks, and submarine volcanic eruptions have caused serious health problems to living organisms and the ecosystems owing to their non-biodegradability, toxicity, and carcinogenicity, persistency, and bioaccumulation (Zou et al. 2016; Fan et al. 2019; Qasem et al. 2021). This problem has also adversely affected human life and sustainable development. Several methods, including ion-exchange, precipitation, oxidation, photocatalysis, separation, and adsorption, have been utilized to eliminate heavy metal ions from polluted water environments (Liu et al. 2015; Ghafoor et al. 2018). Adsorption is considered an outstanding method due to its low investment and operation costs, facile process, high efficiency, and reversibility of the decontamination (Olivera et al. 2016; Yin et al. 2021).

Recently, green sustainable adsorbents derived from natural biomass resources have attracted substantial interests due to their advantages of renewability, non-toxicity, biodegradation, and low cost (Kim et al. 2020). Cellulose (CE) composed of a linear homopolymer linked by β-D, 1, 4 glycosidic bonds is the most abundant biomass type in the world. It has excellent physical and mechanical properties, high stability, and is environmentally friendly (Li et al. 2021). However, the lack of surface chemical activities results in a poor chemical complex, limiting its use as an absorbent of heavy metal ions. Therefore, esterification (Yan et al. 2020), etherification (Hashem et al. 2010), oxidation (Zaccaron et al. 2020), and graft copolymerization (Hou et al. 2020a, b) have been used to functionalize cellulose to improve its adsorption efficiency (Hashem et al. 2020). Chitosan (CS) is a component of the exoskeleton of crustacean marine life and a promising natural adsorptive polymer composed of β-D, 1, 4, glucosamine (Xu et al. 2018). The unique amino and hydroxyl groups existed in CS facilitate the formation of chelates with heavy metal ions (Lakhdhar et al. 2015; Habiba et al. 2017), providing excellent ion binding and adsorptive properties (Wang et al. 2018b). However, CS-based adsorbents, such as CS beads, powder, or flakes, generally have the low adsorption capacity because of their low porosity, protected functional groups, and low mechanical strength and stability (Qasem et al. 2021; Upadhyay et al. 2021), limiting their potential and leading to inefficient regeneration. Hence, chemical modification by cross-linking or grafting has been proposed to alleviate these problems. However, increasing the mechanical strength of CS by combining polymer chains with functional groups comes at the cost of reduced adsorption capacity and increased consumption of chemicals and energy during modification (Vakili et al. 2018; Qasem et al. 2021).

The structure of an absorbent is another crucial factor affecting its adsorption capacity. Porous membranes composed of nanofibers with high specific surface areas and potentially controllable surface properties have gained considerable attention for the efficient removal of heavy metals and other functional products (Awual et al. 2018; Hou et al. 2020a, b; Ma et al. 2021). Electrospinning is currently the most straightforward and most efficient method to produce continuous nanofibers with diameters at micro or nanometers scales (Wang et al. 2017a). These nanofibers have a wide range of utilization due to their unique nanofiber interwoven porous morphology, low carbon footprint, and zero contamination (Tian et al. 2019; Zhang et al. 2022). Tian et al. (2011) prepared a cellulose acetate (CA)/acetone/N, N-dimethylacetamide nanofibers membrane by the way of electrospinning and modification of poly(methacrylic acid). The nanofibers had an average diameter of 750 nm and exhibited high adsorption selectivity for mercury ions. Liu et al. fabricated a ribbon-like porous CA/acetone/dichloromethane composite micro-fibers using electrospinning. The fibers had an average width of 940 nm and pore size of 52 × 98 nm and performed well for copper ion adsorption (Liu et al. 2015). Hamad et al. combined the nanocomposite fibers of pure CA with hydroxyapatite by electrospinning, achieving an excellent separation efficiency of 95.46% within 40 min (Hamad et al. 2020). Fan et al. reported an effective CS/β-cyclodextrin/polyvinyl alcohol (PVA) nanofibrous membrane prepared by electrospinning for the rapid adsorption of

several heavy metal ions (Fan et al. 2019). Karim et al. reported PVA/CS nanofibers membranes fabricated by electrospinning for the selective adsorption of cadmium and lead ions (Karim et al. 2019). Bates et al. designed and fabricated a "sandwich-like" TEMPO-oxidized cellulose/CS-polyethylene oxide (TO-CE/CS-PEO) composite membrane for copper ion adsorption. The porous oxidized cellulose nanofibrils served as the core, and an electrospun nanofibrous membrane consisting of CS-PEO was the outer layer on both sides (Bates et al. 2021).

CE and CS have an excellent biocompatibility together, which has been proved by our previous reports (Xu et al. 2018, 2022). The CE/CS biocomposite nanofibers with the average diameters over 260 nm have been successfully obtained by electrospinning in our team (Wang et al. 2021). Herein, to develop a new-generation green, porous nanofiber adsorption material with a lower nanofiber diameter and the superior adsorption performance. A CA/CS biocomposite ultrafine nanofibrous membrane is prepared by electrospinning and is used for the efficient removal of the aquatic copper ions. The relationships between the parameters of the electrospinning solution, the micro-morphology and porosity, the chemically active sites, and the adsorption capacity of the biocomposite nanofibrous membranes fabricated by conventional and core–shell electrospinning were comprehensively investigated and characterized using a tensiometer, conductometer, scanning electron microscopy (SEM) equipped with an energy dispersive X-ray spectrometry (EDS), transmission electron microscopy (TEM), atomic force microscopy (AFM), specific surface area analyzer, Fourier transform infrared (FTIR) spectroscopy, and X-ray photoelectron spectroscopy (XPS). In addition, the adsorption effects of copper ions, including the initial ion concentration, interaction time, and solution pH, were comparatively analyzed.

Experimental

Materials

Cellulose acetate (CA) was bought from Sinopharm Chemical Reagent Co., Ltd. Chitosan (CS) particles with degree of deacetylation of 90% were obtained from Qindao Huizhi Biological Engineering Co., Ltd. Anhydrous copper sulfate ($CuSO_4$) and bis(cyclohexanone) oxalyldihydrazone (BCO) were bought from Sinopharm Chemical Reagent Co., Ltd. Polyvinyl alcohol (PVA) (M_W = 44,000 g/mol) was provided by Shanghai Taitan Technology Co., Ltd. Glacial acetic acid was purchased from Guangdong Guanghua Technology Co., Ltd. All of them belong to the analytical grade. Deionized water was prepared in our laboratory.

Fabrication of CA/CS biocomposite nonfibrous membrane

CA and CS were dissolved in acetic acid/deionized water at a 60:40 volume ratio with continuous stirring to obtain 3 wt% CA and 3 wt% CS solutions at ambient temperature. The mixed CA/CS solutions were prepared at various mass ratios of CA:CS (10:0, 9:1, 7:3, 5:5, 3:7, 1:9 and 0:10), coded as CA, 10% CS, 30% CS, 50% CS, 70% CS, 90% CS, and CS. 9 wt% PVA solution was added into the CA/CS mixing solution at the weight ratio of 3:7 and mixed by stirring. Subsequently, the solutions were directly used for electrospinning, which avoided the aging effects originating from conformational variation, aggregation, and partial chain scission of chitosan (Sorlier et al. 2002). The CA/CS biocomposite nanofibers with ordinary and core–shell composite structures were prepared by an electrospinning instrument (Elite, Ucalery, China) respectively corresponding to the single and coaxial needles. The grounded negative electrode of the drum was covered with aluminum foil as a receiving device of nanofibers. The electrospinning parameters for the voltage, injection rate, and receiving distance were 15–17 kV, 14–18 cm, and 0.5 mL/min, respectively. The collected CA/CS nanofiber membranes were heated to 240 °C in an air atmosphere for pre-oxidation at a 2 °C/min for 2 h prior to carbonization. The carbonized CA/CS nanofibrous membranes were obtained by heating to 800 °C at a nitrogen atmosphere. The heating rate and holding time were 2 °C/min and 2 h, respectively.

Characterization and measurement

Measurement of surface tension and conductivity of the electrospinning solution

The surface tension test by the method of a Wilhelmy plate were carried out on a tensiometer

(HM301, Guodian, China). The electrical conductivity measurement was performed on a conductometer (DDSJ-318, Cilei, China) at room temperature. Five replicate samples were tested to obtain the average value and the standard deviations.

Micro-morphology of nanofibrous membranes and distribution of copper ions

The micro-morphology of the CA/CS biocomposite nonfibrous membranes was observed by a scanning electron microscopy (SEM) (Hitachi S-3400, Philips, Japan) with an accelerating voltage of 10 kV. Prior to observation, the dried samples were sputter-coated with gold. Energy dispersive X-ray spectrometry (EDS) provided the distribution images of copper ions accompanying with a specific area before and after adsorption. The micro-morphology for core–shell nanofibers was observed using a transmission electron microscopy (TEM) (JEM 2100, JEOL, Japan) at 200 kV accelerating voltage.

Atomic force microscopy (AFM)

Atomic force microscopy (AFM, Bruker Multimode 8) was utilized to evaluate the surface three-dimensional morphology and roughness of the CA/CS biocomposite nanofibrous membranes in a tapping mode. Each sample was observed at a scan range of 6 μm × 6 μm. The roughness of surface was analyzed according to the root average arithmetic roughness (R_a).

N_2 adsorption–desorption isotherms

The N_2 adsorption–desorption isotherms of the CA/CS biocomposite nonfibrous membranes were evaluated by an auto specific surface area analyzer (ASAP 2020, Micromeritics, USA) at a relative pressure of $P/P_0 = 0.99$ and a temperature of 77 K. The specific surface area of samples was calculated according to the Brunauer–Emmett–Teller (BET) method supported by a multilayer adsorption theory. The Barrett–Joyner–Halenda (BJH) model was selected to calculate the distribution of pore size.

Fourier transform infrared (FTIR) spectra

FTIR spectra of the CA/CS biocomposite nonfibrous membranes were collected in the region of 600–4000 cm^{-1} by a Nicolet instrument (IS5, Thermo, USA) equipped with the attenuated total reflectance (ATR) Ge probe.

Thermo-gravimetric analysis (TGA)

The thermal stability of the CA/CS biocomposite nonfibrous membranes with various composite ways was comparatively evaluated using a thermal gravimetric instrument (TG 209-F1, Netzsch, Germany). 5–10 mg samples were heated from 40 to 800 °C under nitrogen atmosphere at a heating rate of 10 °C/min.

Evaluation of heavy metal adsorption

The copper sulfate particles were dissolved in deionized water with constant stirring at room temperature to obtain the copper ion (Cu^{2+}) solutions. The colored Cu^{2+} and BCO reactions were analyzed on an ultraviolet–visible (UV–vis) spectrophotometer. To calculate the concentration of free Cu^{2+} solution, a calibration curve was established. The adsorption measurement was carried out using a conical flask by immersion of specimens. The effects of adsorption parameters including initial concentration of Cu^{2+} (10, 20, 30, 40 mg/L), pH value (1, 2, 3, 4, 5, 6), and adsorption time (0–3000 min) on removal of Cu^{2+} were also investigated. The adsorption capacities of specimens were evaluated following Eq. (1):

$$Q = (C_0 - C_t)V/m \tag{1}$$

where Q is the adsorption capacities of specimens, mg/g; C_0 indicates the initial concentration of copper ions in the testing solution, mg/L; C_t represents the specific concentration of copper ions at any time, mg/L; V is the volume of the testing solution, L; m is the weight of the CA/CS biocomposite nanofibrous membranes, g.

X-ray photoelectron spectrometer (XPS)

The surface chemical compositions of the CA/CS biocomposite nonfibrous membranes were analyzed by a XPS (K-Alpha, Thermo Scientific, USA) with monochromatic Al-Kα. Its scanning step increment for samples was set at 0.1 eV.

Results and discussion

Analysis of surface tension and conductivity

The surface tension and electrical conductivity of the electrospinning solution are the significant parameters affecting the micro-morphology of nanofibers. Figure 1 displays the variation trend of the surface tension and electrical conductivity of the spinning solution at various CA and CS ratios. The conductivity of the electrospinning solution shows an ascending trend as the CS content increases. Specifically, the conductivity increases from 302 to 1370 μs cm^{-1} as the CA to CS ratio decreases from 10:0 to 0:10. The probable reason is that CS dissolution in the acetic acid/water solvents forms ammonium salts, which act as polyelectrolytes, increasing the electrical conductivity of the electrospinning solution (Qasim et al. 2018). The surface tension value decreases slightly from 35.5 to 33.3 mN m^{-1} as the CS content increases from 0 to 30% and then rises back to 34.5 mN m^{-1} as the CS content further increases to 90%. This result demonstrates that the mixing of CA and CS with a low concentration has a negligible effect on the surface tension. Among the biocomposite membranes, the 50% CS group shows the optimum electrospinning performance. In addition to the interaction between the CS and CA macromolecules, CA, CS, and PVA can form hydrogen bonds (Zhang et al. 2007), although the solutions exhibit insufficient entanglement of molecular chains to achieve a critical level for producing fibers at low concentrations (Du and Hsieh 2007).

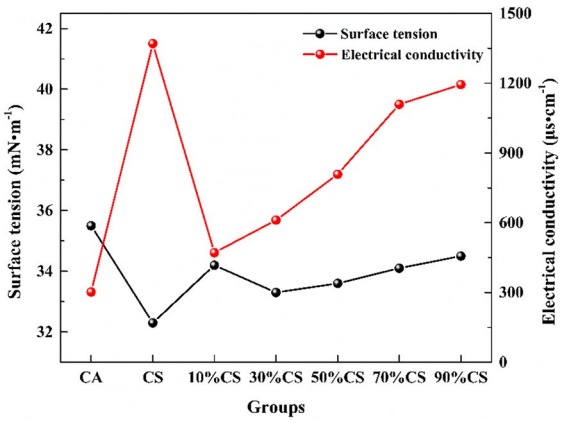

Fig. 1 The surface tension and electrical conductivity of the electrospinning solution at different CA/CS ratios

The morphology of the CA/CS biocomposite nanofibers

The macro- and micro-morphologies and diameters of the CA/CS biocomposite nanofibrous membranes are shown in Fig. 2. The common composite membranes at various CA and CS ratios appeared as porous web-like structures with average nanofibers diameters from 56.22 to 94.39 nm, which is smaller than recently reported bio-based nanofibers (Wang et al. 2017b, 2018a; Yang et al. 2017; Xu et al. 2020). The average diameters initially decrease and then increase as the CS content increases from 10 to 90%. The lowest average diameter of the conventional composite structure is 56.22 nm at 50% CS loading, corresponding to the narrowest diameter distribution. This is attributed to enhance electrostatic forces and reduce surface tension of the resultant solution (Stefanescu et al. 2012). The surfaces of 30% CS and 50% CS membranes are smooth and bead-free. In contrast, an excess amount of CS increases the surface tension of the electrospinning solution, leading to increased nanofiber diameters. Several thinner nanofibers in Fig. 2D, E may be caused by partial deformation and splitting of the charged droplets during electrospinning. The physical adsorption capacity was determined by the porosity and specific surface area. The current CA/CS nanofibers have the smaller diameters than our previously fabricated CE/CS biocomposite nanofibers (Wang et al. 2021), resulting in the higher physical adsorption capacity for copper ions. Additionally, the core–shell biocomposite nanofibrous membrane with CS as the "shell" and CA as the "core" at 30% CS loading can be clearly observed in Fig. 2G. It has a lower average diameter (37.28 nm) but a broader diameter distribution (Fig. 2F) than the 50% CS membrane (Fig. 2C).

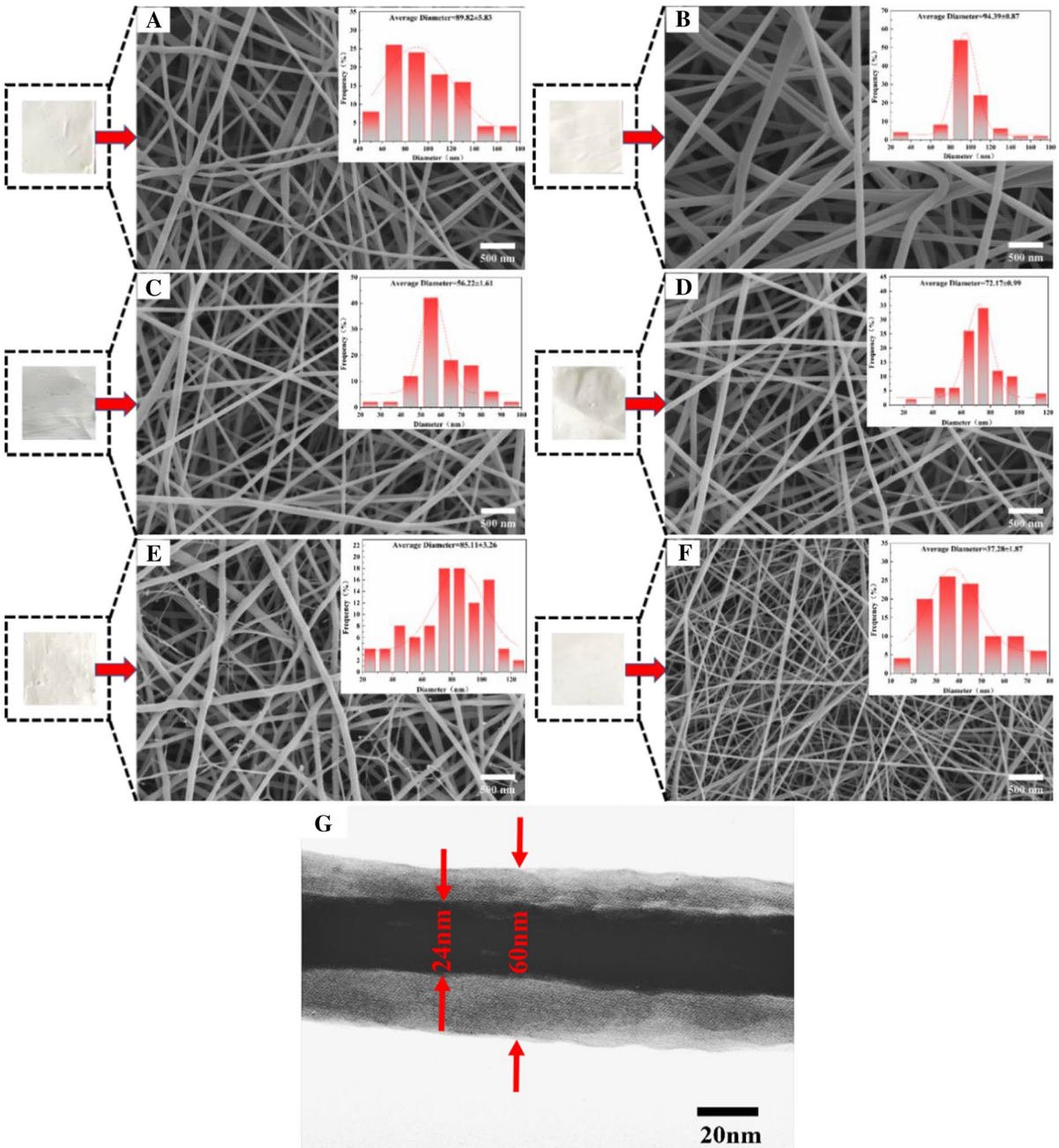

Fig. 2 The macroscopic and microscopic morphologies of the CA/CS biocomposite nanofibrous membranes and their diameters: **A** 10% CS, **B** 30% CS, **C** 50% CS, **D** 70% CS, **E** 90% CS, **F** core–shell 30% CS, **G** TEM image of core–shell structure

The three-dimensional (3D) micro-morphology of the CA/CS biocomposite nanofibrous membranes was further examined by AFM. The nanofibers of the membrane exhibit different diameter distribution and smoothness, consistent with the SEM images. The surface roughness of the nanofibrous membranes was evaluated by analyzing the AFM images with the WSXM software. The detailed pore depth and surface are shown in Fig. 3. A 3D web structure with various interstices was formed by the

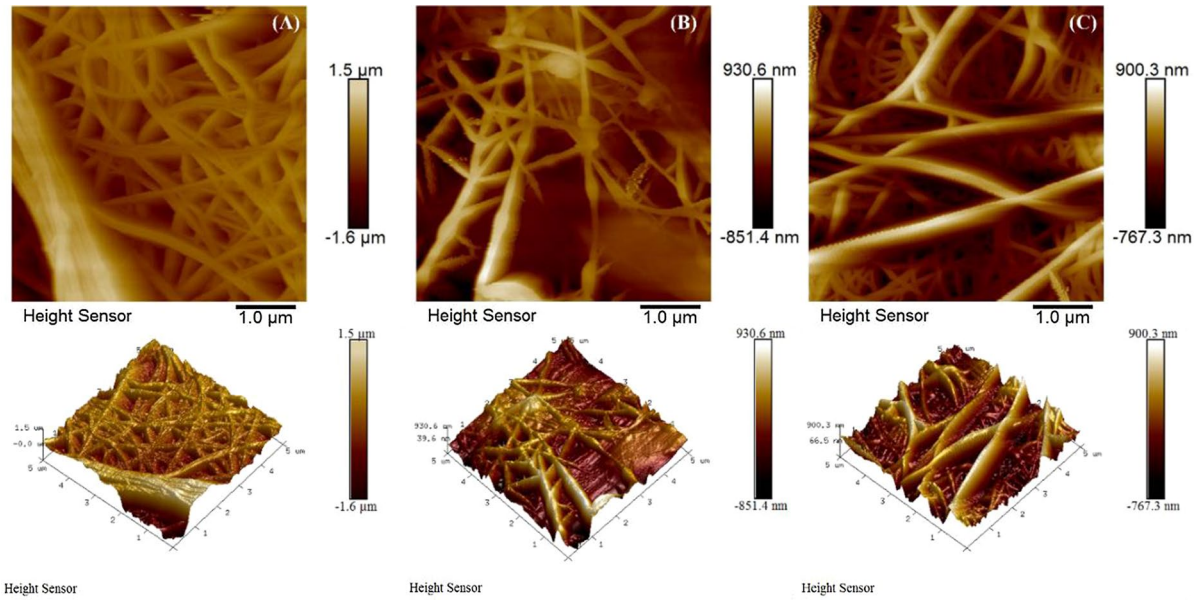

Fig. 3 The AFM of the CA/CS biocomposite nanofibrous membranes: **A** 30% CS, **B** 90% CS, **C** core–shell 30% CS

interconnected ultrafine nanofibers. The 30% CS (306 nm) has a relatively higher R_a than the 90% CS group (195 nm) and the 30% core–shell group (212 nm) because of its larger diameter, more uniform distribution, and smoother nanofibers. Beads and nanofibers mixture are also observed in the 90% CS group. Some inhomogeneous regions of the core–shell membrane and the incorporation of interpenetrating nanofibers may lead to extremely small pore sizes.

Brunauer–Emmet–Teller analysis

The adsorption–desorption curves of N_2 and the pore width distribution of the CA/CS biocomposite nanofibrous membranes are displayed in Fig. 4.

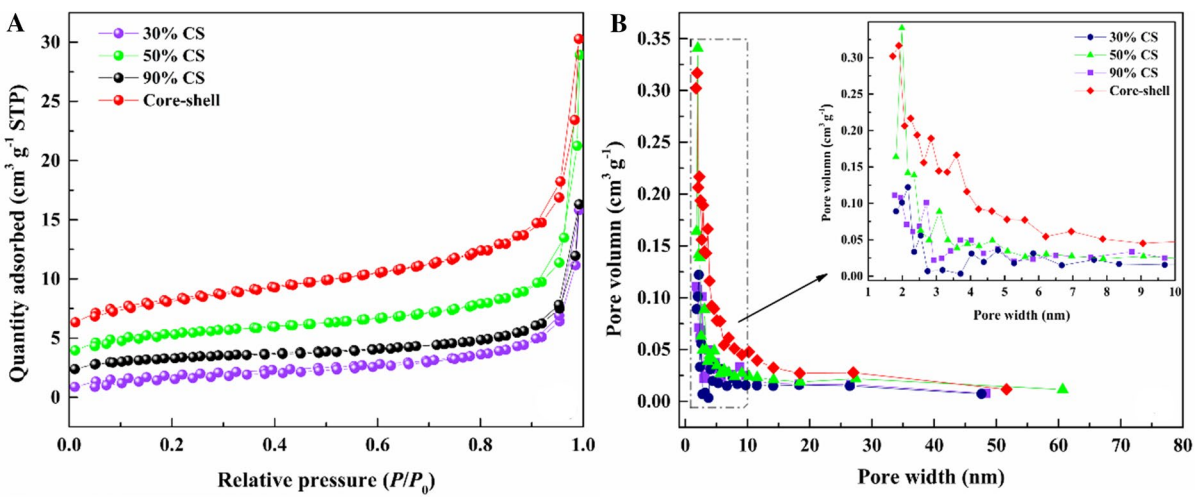

Fig. 4 The N_2 adsorption–desorption isotherms **A**, **B** pore width distribution of the CA/CS biocomposite nanofibrous membranes

Table 1 The porous parameters of CA/CS biocomposite nanofibrous membranes

Samples	BET surface area ($m^2\ g^{-1}$)	Average pore width (nm)	DFT cumulative pore volume ($cm^3\ g^{-1}$)
30%CS	6.65	19.42	0.021
50%CS	8.66	19.03	0.038
90%CS	6.66	16.99	0.023
Core–shell	12.33	11.91	0.036

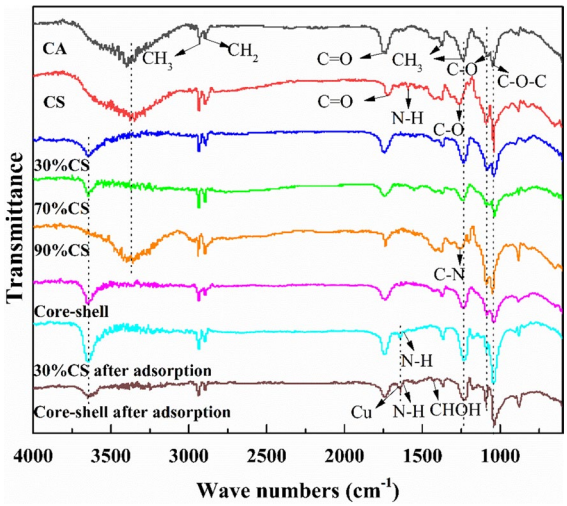

Fig. 5 The FTIR spectra of the CA/CS biocomposite nanofibrous membranes

Figure 4A shows that the curves display typical type-IV profiles with narrow hysteresis loops in the range of 0.8–0.99, especially for the core–shell and 50% CS groups, implying that the mesopores of the specimens, which is in agreement with the pore width distribution in Fig. 4B. Table 1 lists the porosity parameters of the samples. The sample with 30% CS loading exhibits the lowest Brunauer-Emmet-Teller (BET) surface area (6.65 $m^2\ g^{-1}$) but the largest average pore width (19.42 nm). Conversely, the samples with the core–shell composite structure have the highest surface area but the smallest average pore width (11.91 nm). This result correlates well with the micro-morphology observations.

Analysis of FTIR

Figure 5 shows the FTIR spectra of the nanofibrous membranes with the ordinary composite structure at different CA and CS ratios and the core–shell composite nanofibrous membranes before and after adsorption. The adsorption bands at 2936 cm^{-1} and 2896 cm^{-1} are associated with the stretching vibration of CH_3 and CH_2 in both CA and CS, respectively. The 1740 cm^{-1} band is attributed to the stretching vibration of C=O derived from the un-hydrolyzed vinyl acetate group in PVA, the acetyl group in CS, and the carbonyl group in CA (Phan et al. 2019). The adsorption bands at 1370 cm^{-1} and 1230 cm^{-1} are ascribed to the CH_3 acetyl group (Wang et al. 2020). The bands at 1040 cm^{-1} and 1720 cm^{-1} are associated with the C–O–C and C=O stretching vibrations in CS. The band at 1620 cm^{-1} is related to the C–O stretching vibration due to the hydrogen bond between PVA and CS. A relatively weak N–H vibration occurs at 1590 cm^{-1}, it is assigned to the mixed vibration of CS amide II and NH_2 (Li et al. 2012). The broad and strong peaks at 3360 cm^{-1} are –OH and –NH stretching vibrations. As the CS content increases, the absorption band shifts from 3360 cm^{-1} to around 3650 cm^{-1}, indicating that many hydrogen bonds were formed in the composite nanofibers (Koosha and Mirzadeh 2015). The band at 1260 cm^{-1} is related to the C–N bond (Yezer and Demirkol 2020). The amino group characteristic band for the 30% CS and core–shell biocomposite nanofibrous membrane has shifted from 1590 to 1620 cm^{-1}, and an additional peak has occurred at 1640 cm^{-1} after adsorbing copper ion mainly due to the amino group chelation in CS with copper ions (Chen et al. 2019). Thus, both 30% CS and core–shell membranes have superior chemical adsorption for copper ions compared to the other groups. Additionally, two weak peaks are observed at 1430 cm^{-1} and 1090 cm^{-1} corresponding to the bending vibration of CHOH and the out-of-plane bending vibration of C–O in PVA, demonstrating that PVA was still present in the composite nanofibers after exposure to the $CuSO_4$ solution (Ling et al. 2013; Koosha and Mirzadeh 2015).

Analysis of thermal stability

Figure 6 displays the thermogravimetric (TG) and derivative thermogravimetric (DTG) curves of the

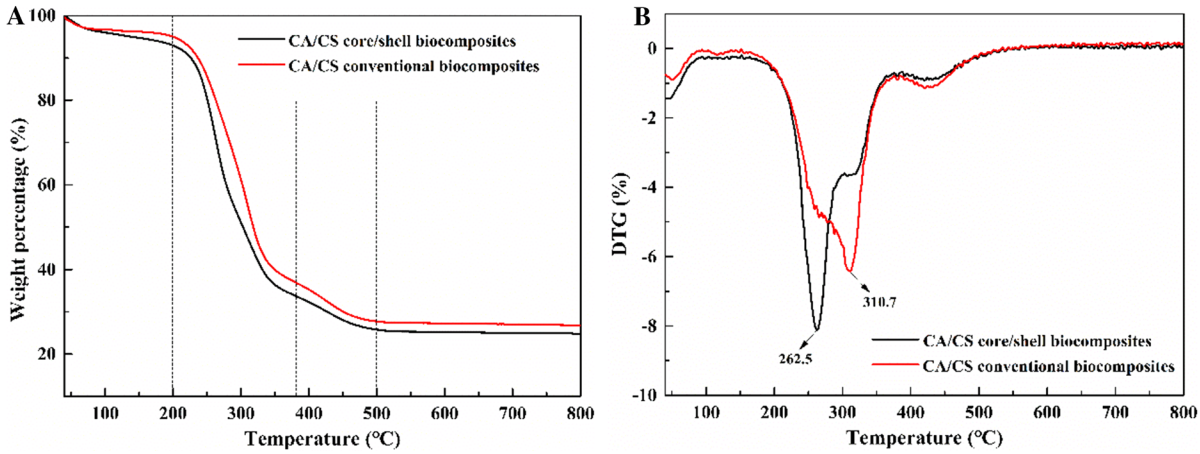

Fig. 6 The TG and DTG curves of the CA/CS biocomposite nanofibrous membranes with core–shell and conventional composite structures

CA/CS biocomposite nanofibrous membranes fabricated by the conventional and the core–shell electrospinning. A 4–5% mass loss below 100 °C can be attributed to the desorption of residual moisture in the samples (Fig. 6A) (Xu et al. 2022). The first major thermal decomposition with a maximum mass loss rate of about 59% between 200 and 380 °C is related to the cleavage of glycosidic linkages of CA and CS via dehydration, deamination, and rearrangement (Pawlak and Mucha 2003; Barud et al. 2008), as well as the dehydration of hydroxyl groups and the formation of the conjugated, unsaturated polyenes in PVA (Rowe et al. 2016). The second major mass loss occurring at 380–500 °C corresponds to the thermal degradation of residual polyene with some volatile organic substances including alkenes, alkanes, and aromatics (Lu et al. 2008). Figure 6B also shows that the maximum thermal decomposition temperature (T_{max}) of the CA/CS biocomposite nanofibrous membranes. The T_{max} is significantly higher for the nanofibers obtained from conventional electrospinning (310.7 °C) than those fabricated by core-shell electrospinning (262.5 °C). This is probably due to that CA has better thermal stability than CS, and the core–shell composite structure with CA as a core and CS as a shell, results in better CS exposure during the heating process, weakening the thermal stability of the CA/CS core–shell biocomposite nanofibers.

Micro-morphology before and after adsorption

The SEM–EDS images of the CA/CS biocomposite nanofibrous membranes after copper ions adsorption are presented in Fig. 7. As observed in Fig. 7A1–A4, many copper particles are evenly adsorbed onto the pure CS, 30% CS, and core–shell nanofibrous membranes, which is confirmed by the EDS images (Fig. 7C1–C4). The pores and gaps of various sizes and irregular shapes contribute to the physical adsorption of copper ions. Figure 7B1 shows that some "cloud-like" thin layers were formed on the pure CS membrane, and the partial enlargement of the image shows that the surface has a dense and rough morphology. The CS nanofibers' excessive aggregation on the surface of the composite membrane after copper ions adsorption prevented the further entry of copper ions into the internal porous network of the membrane, leading to the lowest atomic copper content (0.49%). The many irregular pores on the surface of the 30% CS membrane in Fig. 7A2, B2 are attributed to hydrogen bonding and the van der Waals forces between CS and CA. It is observed in the magnified image that the nanofibers are interwoven and superimposed on each other. The stable porous nanofiber structure results in numerous chemically active sites for the removal of copper ions. The microscopic surface of the core–shell composite membrane is shown in Fig. 7A3, B3.

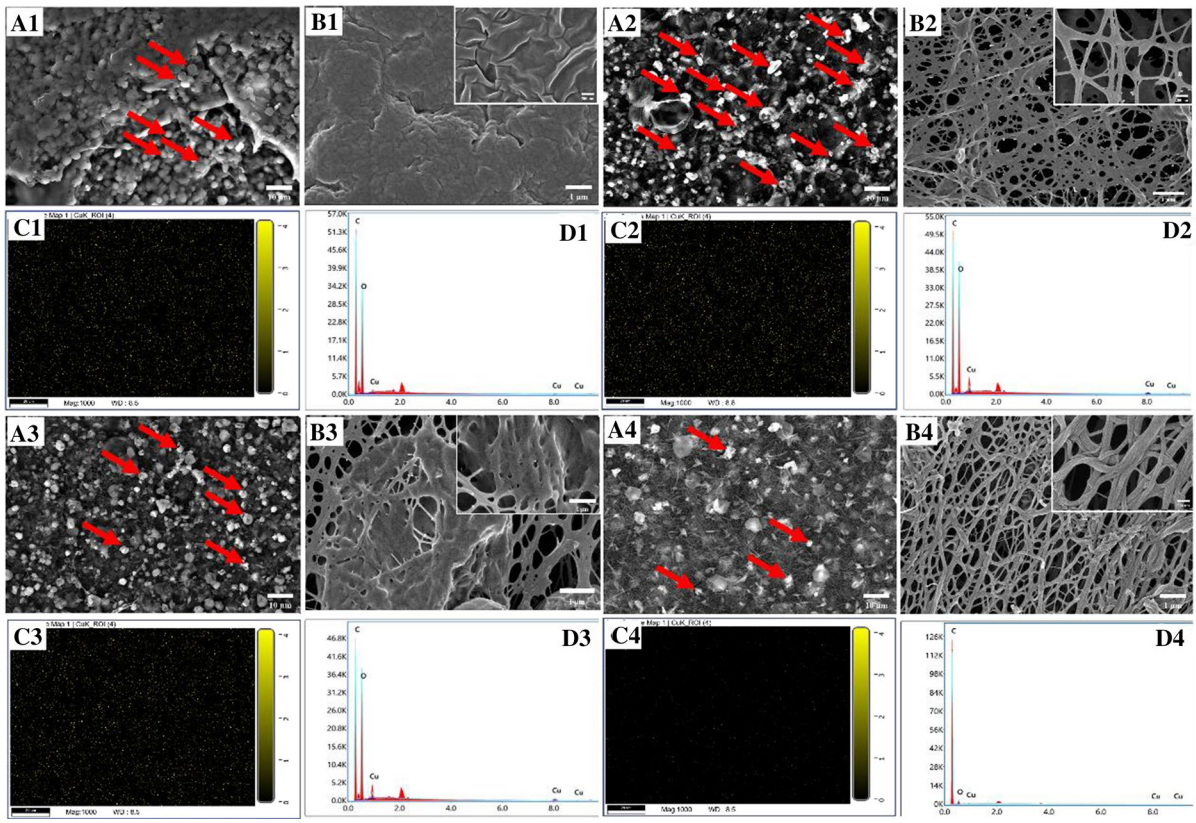

Fig. 7 The SEM–EDS after adsorption of copper ions: **A1**–**D1**. CS, **A2**–**D2**. 30% CS, **A3**–**D3**. Core–shell, **A4**–**D4** 30% CS after carbonization

Some lumps pieces are observed due to the presence of thin nanofibers and many cross-linking sites. After carbonization of the 30% CS composite membrane in Fig. 7A4, B4, the surface fibers were twisted and irregular although the porous structure was not destroyed. The active adsorption sites with specific chemical groups were significantly reduced or disappeared during the carbonization process. Combined with the data in Table 2, it is found that the 30% CS composite membrane adsorbed the highest copper content after adsorption, corresponding to a relative atomic content of 1.85%. The relative atomic copper content of the core–shell composite membranes was slightly lower (1.73%). The atomic copper content of the carbonized 30% CS composite film was only 0.11%, which can be explained by the NH_2 or NH_3^+ groups' destruction and transformation into C–N groups during the carbonization process (Wang et al. 2021).

Table 2 The elemental content of copper after adsorption in the CA/CS biocomposite nanofibrous membranes

Samples	Element	Weight (%)	Atomic (%)
CS	Cu k	2.20	0.49
30% CS	Cu k	7.93	1.85
Core–shell	Cu k	7.45	1.73
Carbonized 30% CS	Cu k	0.56	0.11

Adsorption performance and influencing factors

The adsorption performance of the ultrafine CA/CS biocomposite nanofibrous membranes for copper ions (Cu^{2+}) is shown in Fig. 8. The absorption rate of the nanofibrous membranes with an initial concentration of 30 mg/L continuously increases over time for all groups (Fig. 8A). The absorption rate shows a sharp increase in the initial stage ($t < 30$ min), which is mainly attributed to the large specific surface area

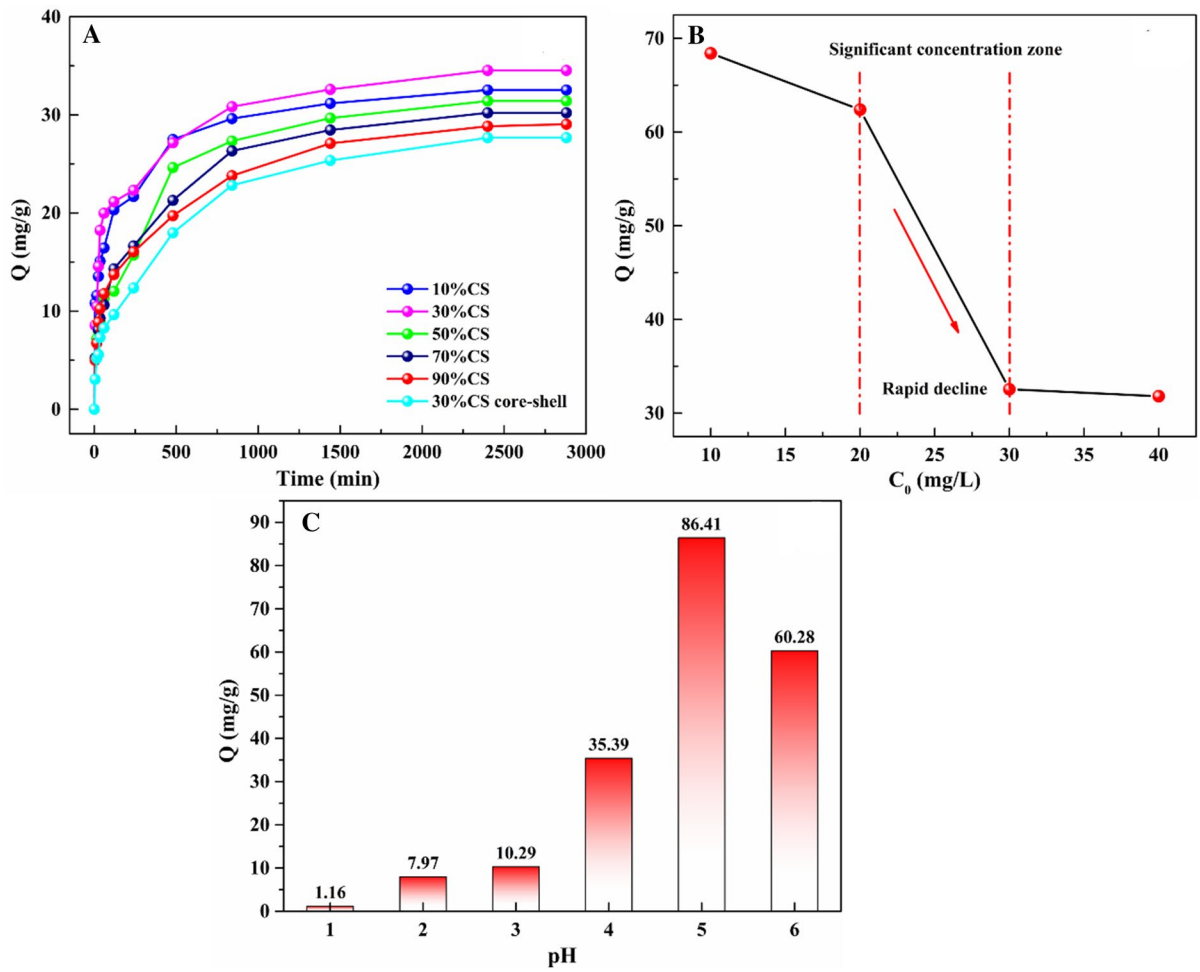

Fig. 8 The adsorption performance of the CA/CS biocomposite nanofibrous membranes: **A** the relation of time and *Q*, **B** the relation of initial concentration and saturated *Q*, **C** the relation of pH and saturated *Q*

with many free adsorption sites on the composite nanofibrous membrane (Bock et al. 2012). The absorption rate slows down and gradually reaches a plateau, which is attributed to a decrease in the Cu^{2+} concentration in the solution and the consumption of adsorption sites. After reaching the equilibrium, the maximum and minimum adsorption rates of the 30% CS ordinary composite and core–shell composite membranes were 34.53 mg/g and 27.67 mg/g, respectively. Moreover, the 30% CS nanofibrous membranes achieved 52.8% of the total adsorption capacity in approximately 30 min. The time to reach the adsorption equilibrium is longer due to the diffusion of Cu^{2+} into the composite nanofiber membrane need take more time.

The adsorption capacity of the 30% CS ordinary composite membrane at different initial concentrations is displayed in Fig. 8B. The adsorption performance decreases with the increasing initial concentration. A significant decline occurs in the concentration range of 20–30 mg/L, corresponding to a 47.8% reduction in the adsorption capacity. The reason is that the total amount of Cu^{2+} in the solution increases with the initial Cu^{2+} concentration, but the number of available active sites on the composite membrane is constant. In addition, a high initial concentration promotes the adsorption and aggregation of Cu^{2+} on the surface layer of the composite membrane, hindering the further diffusion and penetration of Cu^{2+}.

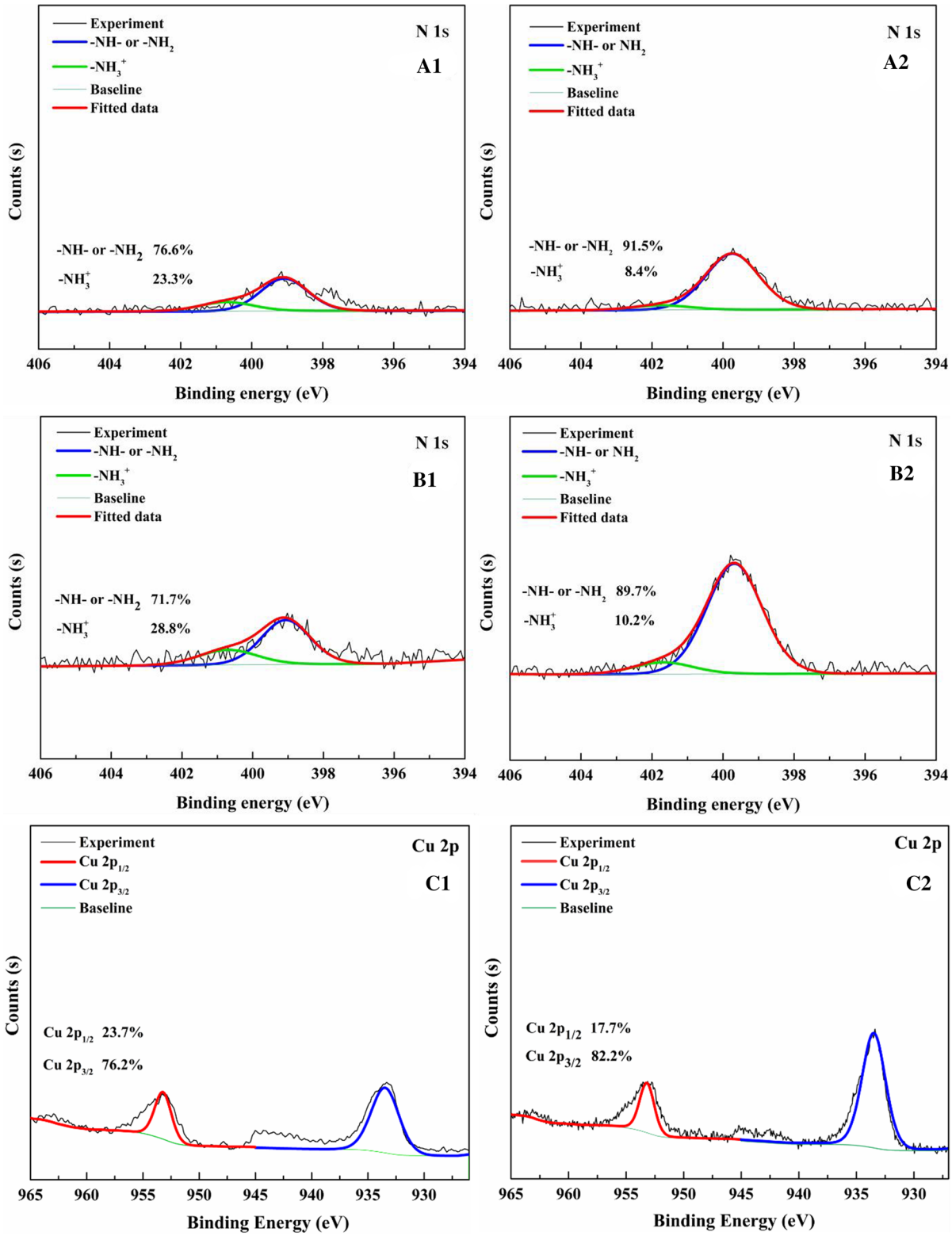
Experiment
-NH- or -NH2
-NH3+
Baseline
Fitted data
N 1s
A1
Counts (s)
-NH- or -NH2 76.6%
-NH3+ 23.3%
406 404 402 400 398 396 394
Binding energy (eV)
Experiment
-NH- or NH2
-NH3+
Baseline
Fitted data
N 1s
A2
Counts (s)
-NH- or -NH2 91.5%
-NH3+ 8.4%
406 404 402 400 398 396 394
Binding energy (eV)
Experiment
-NH- or -NH2
-NH3+
Baseline
Fitted data
N 1s
B1
Counts (s)
-NH- or -NH2 71.7%
-NH3+ 28.8%
406 404 402 400 398 396 394
Binding energy (eV)
Experiment
-NH- or NH2
-NH3+
Baseline
Fitted data
N 1s
B2
Counts (s)
-NH- or -NH2 89.7%
-NH3+ 10.2%
406 404 402 400 398 396 394
Binding energy (eV)
Experiment
Cu 2p1/2
Cu 2p3/2
Baseline
Cu 2p
C1
Counts (s)
Cu 2p1/2 23.7%
Cu 2p3/2 76.2%
965 960 955 950 945 940 935 930
Binding Energy (eV)
Experiment
Cu 2p1/2
Cu 2p3/2
Baseline
Cu 2p
C2
Counts (s)
Cu 2p1/2 17.7%
Cu 2p3/2 82.2%
965 960 955 950 945 940 935 930
Binding Energy (eV)

◂**Fig. 9** The surface chemical compositions of the CA/CS biocomposite nanofibrous membranes: **A1**, **A2** N1s spectra of 30% CS before and after adsorption; **B1**, **B2** N1s spectra of core–shell before and after adsorption; **C1**, **C2** Cu2p spectra of 30% CS and core–shell after adsorption

The pH value of the solution significantly influences the adsorption of heavy metal ions (Guo et al. 2021). The effect of the pH value at the optimum initial concentration of 10 mg/L for the 30% CS ordinary composite membrane on the adsorption performance is illustrated in Fig. 8C. The adsorption performance of the composite membrane increases from 1.16 to 86.41 mg/g as the pH increases from 1 to 5. The optimum adsorption performance is achieved at a pH of 5. This can be explained as the amine groups in CS can protonate either NH_3^+ or $(NH_2–H_3O)^+$ groups at various pH levels of the solution. The copper species were primarily unhydrolyzed Cu^{2+} with some partial $Cu(OH)^+$, and $Cu(OH)_2^{0-}$ in the pH range of 4–6. The protonated amine groups appear to be the predominant active sites for the copper ion adsorption. The coexistence of copper ions and hydrogen ions at low pH values of 1–4 results in competitive adsorption, limiting the reaction of the CS amino groups with Cu^{2+} (Yang et al. 2019). The amino groups of CS formed an ammonium salt that is positively charged and repels the positively charged Cu^{2+} under acidic conditions, reducing its adsorption capacity (Bates et al. 2021). Conversely, the extent of protonation decreases markedly as the pH increases to 6, which leads to the decrease of adsorption capacity (60.28 mg/g) (Hasan et al. 2008).

XPS analysis

XPS analysis was performed before and after adsorption to reveal the mechanism of chemical adsorption on the CA/CS biocomposite nanofibrous membranes with conventional 30% CS and core–shell groups. The XPS spectra are shown in Fig. 9. The surface atomic composition and states are listed in Table 3. There are no changes in the spectra of C1s and O1s in the binding energy position, indicating that the functional groups containing carbon and oxygen did not participate in the copper ion binding reactions. The N1s spectra are shown in Fig. 9A1, A2, B1, B2. The two peaks corresponding to the binding energies of 399.1 and 400.70 eV before copper ion adsorption are related to the $–NH_2$ and the –NH– groups and their protonated $–NH_3^+$ groups in CS (Liu and Bai 2006; Yang et al. 2021; Xie et al. 2021). The two peaks show a significant shift to 399.7 and 401.7 eV after copper ion adsorption, respectively, agreeing with results of previous studies reporting that chemical shifts are significant (Hasan et al. 2006). Therefore, it is verified that the copper ions formed effective chemical coordination complexes with $–NH_2$, –NH–, and the protonated $–NH_3^+$ groups in CS during adsorption probably due to surface bonding formation by sharing lone pairs of electrons in N atoms with the copper ions. This bonding promoted the oxidation states and increased the binding energy of the N atoms (Liu and Bai 2006). The area and width of the peak of –NH or $–NH_2$ after adsorption are larger and narrower after than before the adsorption, which is due to the formation of $Cu[(–NH_2)]_2$ through covalent bonds with the $[Cu–NH_3^+]_2^+$ complex on the surface (Hasan et al. 2008). More covalent bonds were formed in the core–shell samples than in the conventional samples. Nevertheless, the lower binding energy intensity of $–NH_3^+$ for the core–shell membrane may be attributed to the shrinkage of the composite membrane surface with an $–NH_3^+$ enrichment, as seen in Fig. 7B3, preventing the ability to react with the inner active sites and decreasing the adsorption capacity.

The Cu2p spectrum is displayed in Fig. 9C1, C2. Two characteristic peaks corresponding to 932 eV and 952 eV are associated with $Cu2p_{3/2}$ and $Cu2p_{1/2}$, respectively, which proves the effective adsorption of copper ions (Hasan et al. 2006). Although the atomic concentration of $Cu2p_{3/2}$ for core–shell membranes was higher than that of conventional composite membranes, the corresponding adsorption performance was limited by the agglomeration of CS nanofibers on the surface with the blockage of porous network structures as seen in Fig. 7B3. The two additional fluctuations in the 940–946 eV and 961–965 eV regions can be explained as the unsaturated state of the electronic configuration (Hasan et al. 2008). The copper ions may have a coordinated bonding with the amine and hydroxyl groups in CS, and the bonding ability varies with the pH of the solution, the concentration of copper ions, and the CS contents. Combining with above analysis, the adsorption mechanism of the CA/CS biocomposite nanofibrous membranes fabricated by the various electrospinning ways are summarized in Fig. 10.

Table 3 The compositions of surface atomic elements and chemical groups of the CA/CS biocomposite nanofibrous membranes

Composition	30%CS	30%CS after Cu^{2+} -adsorption	Core–shell	Core–shell after Cu^{2+}-adsorption
	Binding energy (eV)		Binding energy (eV)	
–NH– or $–NH_2$	339.09	399.74	339.07	399.68
Atomic concentration (%)	0.67%	1.36%	0.56%	2.05%
$–NH_3^+$	400.70	401.75	400.70	401.68
Atomic concentration (%)	0.20%	0.13%	0.23%	0.24%
Total N1s	0.87%	1.49%	0.79%	2.29%
Cu $2p_{3/2}$	–	933.47	–	933.42
Atomic concentration (%)	0%	0.35%	0%	0.37%
Cu $2p_{1/2}$	–	953.27	–	953.27
Atomic concentration (%)	0%	0.1%	0%	0.1%
Total Cu 2p	0%	0.45%	0%	0.47%

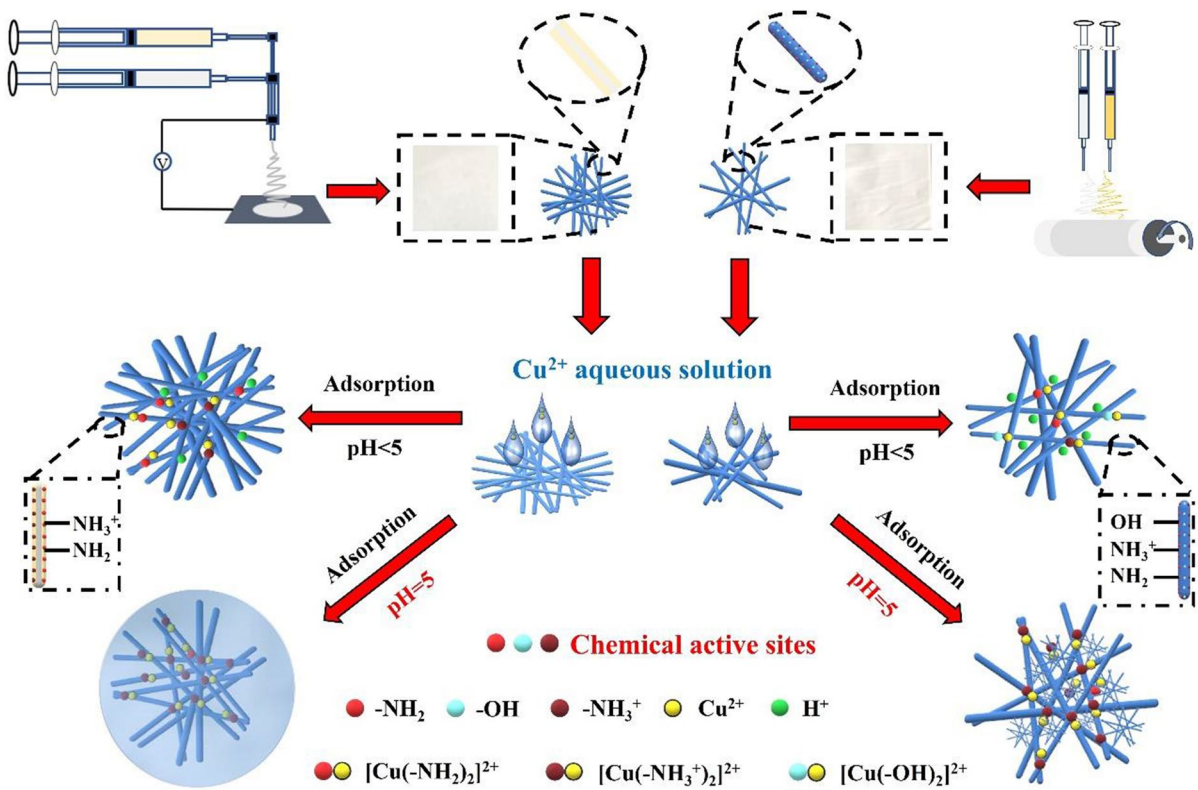

Fig. 10 The adsorption mechanism of the CA/CS biocomposite nanofibrous membranes

Table 4 compares the average diameter and adsorption capacity of the copper ions in this study (ultrafine CA/CS nanofibers) with results of previous reports that used natural CE or CS to fabricate micro- or nano-fibrous membranes including cellulose acetate/chitosan (CA/CS) hollow microfibers, cellulose acetate/silicon dioxide (CA/SiO_2) nanofibers, TEMPO-oxidized cellulose/chitosan/polyethylene oxide (TOC/CS/PEO) sandwich-like nanofibers, cellulose nanocrystals/chitosan (CNC/CS) nanofibers,

Table 4 The average diameter and adsorption capacity of copper ions for various bio-based materials

Cellulose or chitosan-based adsorbents	Chemical reagents or solvents	Average diameter range (nm)	Adsorption capacity of copper ion (mg/g)	References
CA/CS hollow microfibers	Formic acid	600,000–700,000	4.1	Liu and Bai (2005)
CA/SiO_2 nanofibers	Acetone, dimethylacetamide	> 500	23.0	Gebru and Das (2017)
TOC/CS/PEO sandwich-like nanofibers	2,2,6,6-Tetramethylpiperidinooxy, acetic acid	159	36.8	Bates et al. (2021)
CNC/CS nanofibers	Sulfuric acid, acetic acid, poly(vinyl alcohol)	262–498	45.0	Wang et al. (2018a)
CE/CS hydrogel beads	Acetic acid, sodium hydroxide	–	53.2	Li and Bai (2005)
PCF/CS/PEO bi-layer nanofibers	Urea, phosphate ester, acetic acid	372	74.5	Brandes et al. (2020)
CA/CS nanofibers	Trifluoroacetic acid, dichloromethane	450–650	–	Salihu et al. (2012)
CE/CS nanofibers	Trifluoroacetic acid, acetic acid	122–349	80.7	Phan et al. (2019)
CA/CS ultrafine nanofibers	Acetic acid, poly(vinyl alcohol)	37–94	86.4	This study

chitosan/polyethylene oxide (CS/PEO) nanofibers, phosphorylated cellulose/chitosan/polyethylene oxide (PCF/CS/PEO) bi-layer nanofibers, cellulose acetate/chitosan (CA/CS) nanofibers, CE/CS nanofibers, and porous CE/CS hydrogel beads. The results of our study show significantly thinner nanofibers (37–94 nm) and higher adsorption capacity of copper ions (86.4 mg/g) than those of other studies. This can be attributed to the ultrafine nanofiber, the porous and stable structure, and the ideal distribution of chemical adsorption sites. Additionally, the toxic chemical reagents or solvents used in the fabrication of previous CE- or CS-based nanofibers listed in Table 4, such as acetone, dimethylacetamide, 2,2,6,6-tetramethylpiperidinooxy, trifluoroacetic acid, dichloromethane, sulfuric acid and sodium hydroxide, cause the secondary pollution of ecosystems. The current ultrafine CA/CS nanofibrous membrane also has a greener electrospinning solution system (dilute acetic acid/polyvinyl alcohol) and a more facile preparation way without post-treatment, showing a promising prospect for water treatment.

Conclusions

Green, ultrafine CA/CS nanofibrous membranes were successfully fabricated by a facile electrospinning without post-treatment and used for the efficient removal of copper ions from polluted water. The average diameters of the conventional and core–shell ultrafine nanofibers with 50% and 30% CS loading are 56.22 nm and 37.28 nm, respectively. The 30% CS conventional CA/CS biocomposite nanofibrous membranes with a pH = 5 aqueous solution showed the optimum adsorption capacity of copper ions (86.4 mg/g). The core–shell CA/CS biocomposite nanofibrous membranes showed the weaker thermal stability with a 48.2 °C lower maximum thermal decomposition temperature and induced the surface aggregation of more copper ions compared to the conventional one. A more uniform distribution of the -NH_2 or NH_3^+ chemical adsorption sites was obtained by the conventional electrospinning with a single-nozzle needle than by core–shell electrospinning with a coaxial nozzle needle. The former approach had a higher adsorption performance of copper ions and less surface shrinkage of nanofibrous membranes during adsorption. The smart combination of renewable biomass with effective chemical adsorptive sites, the electrospinning technology that produces an interwoven porous structure, and an adsorption method with low cost and a facile operation resulted in high removal efficiency of heavy metals from polluted aqueous media to improve water sustainability and availability for human and other living organisms.

Acknowledgments The authors sincerely appreciated the financial support of the Applied Basic Research Programs of Yunnan Province (The mechanical fibrillation mechanism of bamboo-based cellulose nanofibrils with green low energy consumption, 202201AT070058), the Opening Project of Guangxi Key Laboratory of Forest Products Chemistry and Engineering (GXFK2209), the National Natural Science Foundation of China (NSFC) (32060381), the Applied Basic Research Programs of Yunnan Province (The fabrication of biomass porous nanocomposite fiber for adsorption functional membrane and synergistic mechanism of network hinge, 2019FB067), the Scientific Research Funds of Educational Committee of Yunnan Province (2022Y552), National College Students Innovation and Entrepreneurship Training Program (202110677009), the High Level Innovative One-Ten-Thousand Youth Talents of Yunnan Province (YNWR-QNBJ-2020-203), the USDA National Institute of Food and Agriculture (1012359) and 111 Project (D21027).

Author contributions KX and SW proposed the scientific target and designed the experiments. QL, GS and RL helped to complete the operations and data collection of tensiometer, conductometer and FTIR instruments. LX and JY helped to do the analyses of curves in XPS and BET. GD and JZ and provided lots of help in discussing the relations among parameters of electrospun solution, micro-morphology and porosity for nanofibers, the variation of chemical active sites and adsorption performance of biocomposite nanofibrous membranes for conventional and core–shell electrospinning as well as the adsorption effect factors of copper ions. JW was responsible for completing all the other experiments and wrote the original draft. ZT polished the English grammar, and SW further revised the manuscript. KX and SW provided the funds support.

Declarations

Competing interests The authors have not disclosed any competing interests.

References

Awual MR, Khraisheh M, Alharthi NH, Luqman M, Islam A, Karim MR, Rahman MM, Khaleque MA (2018) Efficient detection and adsorption of cadmium (II) ions using innovative nano-composite materials. Chem Eng J 343:118–127. https://doi.org/10.1016/j.cej.2018.02.116

Barud HS, de Araújo Júnior AM, Santos DB, de Assunção RMN, Meireles CS, Cerqueira DA, Filho GR, Ribeiro CA, Messaddeq Y, Ribeiro SJL (2008) Thermal behavior of cellulose acetate produced from homogeneous acetylation of bacterial cellulose. Thermochim Acta 471:61–69. https://doi.org/10.1016/j.tca.2008.02.009

Bates IIC, Loranger É, Mathew AP, Chabot B (2021) Cellulose reinforced electrospun chitosan nanofibers biobased composite sorbent for water treatment applications. Cellulose 28:4865–4885. https://doi.org/10.1007/s10570-021-03828-4

Bock N, Dargaville TR, Woodruff MA (2012) Electrospraying of polymers with therapeutic molecules: state of the art. Prog Polym Sci 37:1510–1551. https://doi.org/10.1016/j.progpolymsci.2012.03.002

Brandes R, Brouillette F, Chabot B (2020) Phosphorylated cellulose/electrospun chitosan nanofibers media for removal of heavy metals from aqueous solutions. J Appl Polym Sci 138:50021. https://doi.org/10.1002/app.50021

Chen Q, Zheng JW, Wen LY, Yang C, Zhang LJ (2019) A multi-functional group modified cellulose for enhanced heavy metal cadmium adsorption: performance and quantum chemical mechanism. Chemosphere 224:509–518. https://doi.org/10.1016/j.chemosphere.2019.02.138

Cheng XQ, Li S, Bao H, Yang X, Li Z, Zhang Y, Wang K, Ma J, Ullah A, Shao L (2021) Poly(sodium-p-styrenesulfonate)-grafted UiO-66 composite membranes boosting highly efficient molecular separation for environmental remediation. Adv Compos Hybrid Mater 4:562–573. https://doi.org/10.1007/s42114-021-00253-w

Du J, Hsieh YL (2007) PEGylation of chitosan for improved solubility and fiber formation via electrospinning. Cellulose 14:543–552. https://doi.org/10.1007/s10570-007-9122-3

Fan JP, Luo JJ, Zhang XH, Zhen B, Dong CY, Li YC, Shen J, Cheng YT, Cheng HP (2019) A novel electrospun β-CD/CS/PVA nanofiber membrane for simultaneous and rapid removal of organic micropollutants and heavy metal ions from water. Chem Eng J 378:122232. https://doi.org/10.1016/j.cej.2019.122232

Gebru KA, Das C (2017) Removal of Pb (II) and Cu (II) ions from wastewater using composite electrospun cellulose acetate/titanium oxide (TiO_2) adsorbent. J Water Process Eng 16:1–13. https://doi.org/10.1016/j.jwpe.2016.11.008

Ghafoor S, Hussain SZ, Waseem S, Arshad SN (2018) Photoreduction of heavy metal ions and photo-disinfection of pathogenic bacteria under simulated solar light using photosensitized TiO_2 nanofibers. RSC Adv 8:20354–20362. https://doi.org/10.1039/C8RA01237G

Guo L, Zhang Y, Zheng J, Shang L, Shi Y, Wu Q, Liu X, Wang Y, Shi L, Shao Q (2021) Synthesis and characterization of ZnNiCr-layered double hydroxides with high adsorption activities for Cr(VI). Adv Compos Hybrid Mater 4:819–829. https://doi.org/10.1007/s42114-021-00260-x

Habiba U, Afifi AM, Salleh A, Ang BC (2017) Chitosan/(polyvinyl alcohol)/zeolite electrospun composite nanofibrous membrane for adsorption of Cr^{6+}, Fe^{3+} and Ni^{2+}. J Hazard Mater 322:182–194. https://doi.org/10.1016/j.jhazmat.2016.06.028

Hamad AA, Hassouna MS, Shalaby TI, Elkady MF, Abd Elkawi MA, Hamad HA (2020) Electrospun cellulose acetate nanofiber incorporated with hydroxyapatite for removal of heavy metals. Int J Biol Macromol 151:1299–1313. https://doi.org/10.1016/j.ijbiomac.2019.10.176

Hasan S, Krishnaiah A, Ghosh TK, Viswanath DS, Boddu VM, Smith ED (2006) Adsorption of divalent cadmium (Cd (II)) from aqueous solutions onto chitosan-coated perlite beads. Ind Eng Chem Res 45:5066–5077. https://doi.org/10.1021/ie0402620

Hasan S, Ghosh TK, Viswanath DS, Boddu VM (2008) Dispersion of chitosan on perlite for enhancement of copper (II)

adsorption capacity. J Hazard Mater 152:826–837. https://doi.org/10.1016/j.jhazmat.2007.07.078

Hashem A, Azzeer AM, Ayoub A (2010) The removal of Hg (II) Ions from laboratory wastewater onto phosphorylated haloxylon ammodendron: kinetic and equilibrium studies. Polym-Plast Technol 49:1463–1472. https://doi.org/10.1080/03602559.2010.496423

Hashem A, Fletcher AJ, Younis H, Mauof H, Abou-Okeil A (2020) Adsorption of Pb(II) ions from contaminated water by 1,2,3,4-butanetracarboxylic acid-modified microcrystalline cellulose: isotherms, kinetics, and thermodynamic studies. Int J Biol Macromol 164:3193–3203. https://doi.org/10.1016/j.ijbiomac.2020.08.159

Hou DF, Liu ZY, Zhou L, Tan H, Yang W, Yang MB (2020) A facile strategy towards heterogeneous preparation of thermoplastic cellulose grafted polyurethane from amorphous regenerated cellulose paste. Int J Biol Macromol 161:177–186. https://doi.org/10.1016/j.ijbiomac.2020.05.203

Hou C, Wang B, Murugadoss V, Vupputuri S, Chao Y, Guo Z, Wang C, Du W (2020) Recent advances in Co_3O_4 as anode materials for high-performance lithium-ion batteries. Eng Sci 11:19–30

Karim MR, Aijaz MO, Alharth NH, Alharbi HF, Al-Mubaddel FS, Awual MR (2019) Composite nanofibers membranes of poly (vinyl alcohol)/chitosan for selective lead (II) and cadmium (II) ions removal from wastewater. Ecotox Environ Safe 169:479–486. https://doi.org/10.1016/j.ecoenv.2018.11.049

Kim S, Par YH, Lee JB, Kim HS, Choi YE (2020) Phosphorus adsorption behavior of industrial waste biomass-based adsorbent, esterified polyethylenimine-coated polysulfone-*Escherichia coli* biomass composite fibers in aqueous solution. J Hazard Mater 400:123217. https://doi.org/10.1016/j.jhazmat.2020.123217

Koosha M, Mirzadeh H (2015) Electrospinning, mechanical properties, and cell behavior study of chitosan/PVA nanofibers. J Biomed Mater Res A 103:3081–3093. https://doi.org/10.1002/jbm.a.35443

Lakhdhar I, Mangin P, Chabot B (2015) Copper (II) ions adsorption from aqueous solutions using electrospun chitosan/PEO nanofibres: effects of process variables and process optimization. J Water Process Eng 7:295–305. https://doi.org/10.1016/j.jwpe.2015.07.004

Li N, Bai R (2005) Copper adsorption on chitosan-cellulose hydrogel beads: behaviors and mechanisms. Sep Purif Technol 42:237–247. https://doi.org/10.1016/j.seppur.2004.08.002

Li W, Li XY, Wang T, Li XX, Pan SY, Deng HB (2012) Nanofibrous mats layer-by-layer assembled via electrospun cellulose acetate and electrosprayed chitosan for cell culture. Eur Polym J 48:1846–1853. https://doi.org/10.1016/j.eurpolymj.2012.08.001

Li T, Chen CJ, Brozena AH, Zhu JY, Xu LX, Driemeier C, Dai JQ, Rojas OJ, Isogai A, Wagberg L, Hu LB (2021) Developing fibrillated cellulose as a sustainable technological material. Nature 590:47–56. https://doi.org/10.1038/s41586-020-03167-7

Ling S, Qi Z, Knight DP, Shao Z, Chen X (2013) FTIR imaging, a useful method for studying the compatibility of silk fibroin-based polymer blends. Polym Chem 4:5401–5406. https://doi.org/10.1039/C3PY00508A

Liu CX, Bai RB (2005) Preparation of chitosan/cellulose acetate blend hollow fibers for adsorptive performance. J Membr Sci 267:68–77. https://doi.org/10.1016/j.memsci.2006.07.045

Liu CX, Bai RB (2006) Adsorptive removal of copper ions with highly porous chitosan/cellulose acetate blend hollow fiber membranes. J Membr Sci 284:313–322. https://doi.org/10.1016/j.memsci.2006.07.045

Liu RL, Tang CY, Zhao JY, Liu HQ (2015) Electrospun membranes of nanoporous structure cellulose acetate and its adsorptive behaviors using Copper(II) as models. Desalin Water Treat 56:1768–1775. https://doi.org/10.1080/19443994.2014.958108

Lu J, Wang T, Drzal LT (2008) Preparation and properties of microfibrillated cellulose polyvinyl alcohol composite materials. Compos Part A Appl Sci Manuf 39:738–746

Ma Y, Xie X, Yang W, Yu Z, Sun X, Zhang Y, Yang X, Kimura H, Hou C, Guo Z, Du W (2021) Recent advances in transition metal oxides with different dimensions as electrodes for high-performance supercapacitors. Adv Compos Hybrid Mater 4:906–924. https://doi.org/10.1007/s42114-021-00358-2

Olivera S, Muralidhara HB, Venkatesh K, Guna VK, Gopalakrishna K, Kumar KY (2016) Potential applications of cellulose and chitosan nanoparticles/composites in wastewater treatment: a review. Carbohyd Polym 153:600–618. https://doi.org/10.1016/j.carbpol.2016.08.017

Pawlak A, Mucha M (2003) Thermogravimetric and FTIR studies of chitosan blends. Thermochim Acta 396:153–166. https://doi.org/10.1016/S0040-6031(02)00523-3

Phan DN, Lee H, Huang BJ, Mukai Y, Kim IS (2019) Fabrication of electrospun chitosan/cellulose nanofibers having adsorption property with enhanced mechanical property. Cellulose 26:1781–1793. https://doi.org/10.1007/s10570-018-2169-5

Qasem NAA, Mohammed RH, Lawal DU (2021) Removal of heavy metal ions from wastewater: a comprehensive and critical review. NPJ Clean Water 4:1–15. https://doi.org/10.1038/s41545-021-00127-0

Qasim SB, Zafar MS, Najeeb S, Khurshid Z, Shah AH, Husain S, Rehman IU (2018) Electrospinning of chitosan-based solutions for tissue engineering and regenerative medicine. Int J Mol Sci 19:407. https://doi.org/10.3390/ijms19020407

Rowe AA, Tajvidi M, Gardner DJ (2016) Thermal stability of cellulose nanomaterials and their composites with polyvinyl alcohol (PVA). J Therm Anal Calorim 126:1371–1386. https://doi.org/10.1007/s10973-016-5791-1

Salihu G, Goswami P, Russell S (2012) Hybrid electrospun nonwovens from chitosan/cellulose acetate. Cellulose 19:739–749. https://doi.org/10.1007/s10570-012-9666-8

Sorlier P, Viton C, Domard A (2002) Relation between solution properties and degree of acetylation of chitosan: role of aging. Biomacromol 3:1336–1342. https://doi.org/10.1021/bm0256146

Stefanescu C, Daly WH, Negulescu II (2012) Biocomposite films prepared from ionic liquid solutions of chitosan and cellulose. Carbohyd Polym 87:435–443. https://doi.org/10.1016/j.carbpol.2011.08.003

Sun J, Mu Q, Kimura H, Murugadoss V, He M, Du W, Hou C (2022) Oxidative degradation of phenols and substituted phenols in the water and atmosphere: a review. Adv Compos Hybrid Mater. https://doi.org/10.1007/s42114-022-00435-0

Tian Y, Wu M, Liu RG, Li YX, Wang DQ, Tan JJ, Wu RC, Huang Y (2011) Electrospun membrane of cellulose acetate for heavy metal ion adsorption in water treatment. Carbohyd Polym 83:743–748. https://doi.org/10.1016/j.carbpol.2010.08.054

Tian HF, Yuan L, Wang JG, Wu H, Wang HL, Xiang AM, Ashok B, Rajulu AV (2019) Electrospinning of polyvinyl alcohol into crosslinked nanofibers: an approach to fabricate functional adsorbent for heavy metals. J Hazard Mater 378:120751. https://doi.org/10.1016/j.jhazmat.2019.120751

Upadhyay U, Sreedhar I, Singh SA, Patel CM, Anitha KL (2021) Recent advances in heavy metal removal by chitosan based adsorbents. Carbohyd Polym 251:117000. https://doi.org/10.1016/j.carbpol.2020.117000

Vakili M, Deng S, Li T, Wang W, Wang WJ, Yu G (2018) Novel crosslinked chitosan for enhanced adsorption of hexavalent chromium in acidic solution. Chem Eng J 347:782–790. https://doi.org/10.1016/j.cej.2018.04.181

Wang GL, Yu DM, Kelkar AD, Zhang LF (2017a) Electrospun nanofiber: Emerging reinforcing filler in polymer matrix composite materials. Prog Polym Sci 75:73–107. https://doi.org/10.1016/j.progpolymsci.2017.08.002

Wang LH, Yang H, Hou JZ, Zhang WX, Xiang CH, Li LL (2017b) Effect of the electrical conductivity of core solutions on the morphology and structure of core–shell CA-PCL/CS nanofibers. New J Chem 41:15072–15078. https://doi.org/10.1039/c7nj02805a

Wang D, Cheng WL, Yue YY, Xuan LH, Ni XH, Han GP (2018a) Electrospun cellulose nanocrystals/chitosan/polyvinyl alcohol nanofibrous films and their exploration to metal ions adsorption. Polymers 10:1046. https://doi.org/10.3390/polym10101046

Wang HX, Qian J, Ding FY (2018b) Emerging chitosan-based films for food packaging applications. J Agric Food Chem 66:395–413. https://doi.org/10.1021/acs.jafc.7b04528

Wang Y, Wu JQ, Wan Q, Zhang L, Lei HN (2020) Preparation of chitosan/polyvinyl alcohol electrospinning nano-membranes using the green solvent, plasma acid. J Macromol Sci B 59:731–746. https://doi.org/10.1080/00222348.2020.1800921

Wang ZH, Kang KY, Wu JX, Hu Q, Harper DP, Du GB, Wang SQ, Xu KM (2021) Comparative effects of electrospinning ways for fabricating green, sustainable, flexible, porous, nanofibrous cellulose/chitosan carbon mats as anode materials for lithium-ion batteries. J Mater Res Technol 11:50–61. https://doi.org/10.1016/j.jmrt.2021.01.009

Xie P, Liu Y, Feng M, Niu M, Liu C, Wu N, Sui K, Patil RR, Pan D, Guo Z, Fan R (2021) Hierarchically porous Co/C nanocomposites for ultralight high-performance microwave absorption. Adv Compos Hybrid Mater 4:173–185. https://doi.org/10.1007/s42114-020-00202-z

Xu KM, Liu C, Kang KY, Zheng ZF, Wang SQ, Tang ZG, Yang WX (2018) Isolation of nanocrystalline cellulose from rice straw and preparation of its biocomposites with chitosan: physicochemical characterization and evaluation of interfacial compatibility. Compos Sci Technol 154:8–17. https://doi.org/10.1016/j.compscitech.2017.10.022

Xu Q, Peng J, Zhang WX, Wang XJ, Lou T (2020) Electrospun cellulose acetate/P (DMDAAC-AM) nanofibrous membranes for dye adsorption. J Appl Polym Sci 137:48565. https://doi.org/10.1002/app.48565

Xu KM, Li QS, Xie LK, Shi ZJ, Su GM, Harper D, Tang ZG, Zhou JY, Du GB, Wang SQ (2022) Novel flexible, strong, thermal-stable, and high-barrier switchgrass-based lignin-containing cellulose nanofibrils/chitosan biocomposites for food packaging. Ind Crop Prod 179:114661. https://doi.org/10.1016/j.indcrop.2022.114661

Yan GH, Chen BL, Zheng XH, Sun Y, Tan X, Lin L (2020) Recent advances on sustainable cellulosic materials for pharmaceutical carrier applications. Carbohyd Polym 244:116492. https://doi.org/10.1016/j.carbpol.2020.116492

Yang WQ, Sousa AMM, Fan XT, Jin T, Li XH, Tomasula PM, Liu LS (2017) Electrospun ultra-fine cellulose acetate fibrous mats containing tannic acid-Fe^{3+} complexes. Carbohyd Polym 157:1173–1179. https://doi.org/10.1016/j.carbpol.2016.10.078

Yang DX, Li LF, Chen BL, Shi SX, Nie J, Ma GP (2019) Functionalized chitosan electrospun nanofiber membranes for heavy-metal removal. Polymer 163:74–85. https://doi.org/10.1016/j.polymer.2018.12.046

Yang BB, Gu KF, Wang SH, Yi Z, Zhou Y, Gao CJ (2021) Chitosan nanofiltration membranes with gradient cross-linking and improved mechanical performance for the removal of divalent salts and heavy metal ions. Desalination 516:115200. https://doi.org/10.1016/j.desal.2021.115200

Yezer I, Demirkol DO (2020) Cellulose acetate–chitosan based electrospun nanofibers for bio-functionalized surface design in biosensing. Cellulose 27:10183–10197. https://doi.org/10.1007/s10570-020-03486-y

Yin C, Wang C, Hu Q (2021) Selective removal of As(V) from wastewater with high efficiency by glycine-modified Fe/Zn-layered double hydroxides. Adv Compos Hybrid Mater 4:360–370. https://doi.org/10.1007/s42114-021-00214-3

Zaccaron S, Henniges U, Potthast A, Rosenau T (2020) How alkaline solvents in viscosity measurements affect data for oxidatively damaged cellulose. Cuoxam Cadoxen Carbohyd Polym 240:116251. https://doi.org/10.1016/j.carbpol.2020.116251

Zhang YY, Huang XB, Duan B, Wu LL, Li S, Yuan XY (2007) Preparation of electrospun chitosan/poly (vinyl alcohol) membranes. Colloid Polym Sci 285:855–863. https://doi.org/10.1007/s00396-006-1630-4

Zhang Z, Zhao Y, Li Z, Zhang L, Liu Z, Long Z, Li Y, Fan R, Sun K, Zhang Z (2022) Synthesis of carbon/SiO_2 core-sheath nanofibers with Co-Fe nanoparticles embedded in via electrospinning for high-performance microwave absorption. Adv Compos Hybrid Mater 5:513–524. https://doi.org/10.1007/s42114-021-00350-w

Zou YD, Wang XX, Khan A, Wang PY, Liu YH, Alsaedi A, Hayat T, Wang XK (2016) Environmental remediation and application of nanoscale zero-valent iron and its composites for the removal of heavy metal ions: a review. Environ Sci Technol 50:7290–7304. https://doi.org/10.1021/acs.est.6b01897

Wang ZH, Kang KY, Wu JX, Hu Q, Harper DP, Du GB, Wang SQ, Xu KM (2021) Comparative effects of electrospinning ways for fabricating green sustainable flexible porous nanofibrous cellulose/chitosan carbon mats

as anode materials for lithium-ion batteries. Journal of Materials Research and Technology 1150-61 10.1016/j.jmrt.2021.01.009